

“Keep on ROCKIn”: Repurposed ROCK inhibitors to boost corneal endothelial regeneration

Hendrik Vercammen^{a,b,d}, Martin Ondra^{c,e}, Jana Kotulova^c, Edgar Cardenas De La Hoz^f, Charissa Witters^{a,b,d}, Katerina Jecmenova^c, Maxim Le Compte^d, Christophe Deben^d, Sorcha Ní Dhubhghaill^g, Carina Koppen^{a,b}, Marián Hajdúch^{c,e}, Bert Van den Bogerd^{c,e,*}

^a Antwerp Research Group for Ocular Science (ARGOS), Translational Neurosciences, Faculty of Medicine and Health Sciences, University of Antwerp, Wilrijk, Belgium

^b Department of Ophthalmology, Antwerp University Hospital, Edegem, Belgium

^c Institute of Molecular and Translational Medicine, Faculty of Medicine and Dentistry, Palacky University Olomouc, Olomouc, Czech Republic

^d DrugVision Lab, University of Antwerp, Wilrijk, Belgium

^e Czech Advanced Technology and Research Institute (CATRIN), Palacky University Olomouc, Olomouc, Czech Republic

^f Industrial Vision Lab, University of Antwerp, Wilrijk, Belgium

^g Department of Ophthalmology, Brussels University Hospital, Jette, Belgium

ARTICLE INFO

Keywords:

Drug repurposing
Small molecule screening
ROCK inhibitors
Corneal endothelial regeneration
Chroman-1

ABSTRACT

The global shortage of corneal endothelial graft tissue necessitates the exploration of alternative therapeutic strategies. Rho-associated protein kinase inhibitors (ROCKi), recognized for their regenerative potential in cardiology, oncology, and neurology, have shown promise in corneal endothelial regeneration. This study investigates the repurposing potential of additional ROCKi compounds. Through screening a self-assembled library of ROCKi on B4G12 corneal endothelial cells, we evaluated their dose-dependent effects on proliferation, migration, and toxicity using live-cell imaging. Nine ROCKi candidates significantly enhanced B4G12 proliferation compared to the basal growth rate. These candidates were further assessed for their potential to accelerate wound closure as another indicator for tissue regeneration capacity, with most demonstrating notable efficacy. To assess the potential impact of candidate ROCKi on key corneal endothelial cell markers related to cell proliferation, leaky tight junctions and ion efflux capacity, we analyzed the protein expression of cyclin E1, CDK2, p16, ZO-1 and Na⁺/K⁺-ATPase, respectively. Immunocytochemistry and western blot analysis confirmed the preservation of corneal endothelial markers post-treatment with ROCKi hits. However, notable cytoplasm enlargement and nuclear fragmentation were detected after the treatment with SR-3677 and Thiazovivin,

Abbreviations: Abl, ABL proto-oncogene 1, non-receptor tyrosine kinase; ALCAM, Activated leukocyte cell adhesion molecule; AMPK, 5' AMP-activated protein kinase; ANOVA, Analysis of variance; ATMP, Advanced therapy medicinal product; AUC, Area under the curve; Aurora A, Aurora kinase A; B4G12, Immortalized corneal endothelial cell line; BCA, Bicinchoninic acid; BFGF, Basic fibroblast growth factor; BSA, Bovine serum albumin; CaMKII, Ca²⁺/calmodulin-dependent protein kinase II; CaMKIIa, Ca²⁺/calmodulin-dependent protein kinase IIa; CCNE1, Cyclin E1; CDK2, Cyclin-dependent kinase 2; CEnCs, Corneal endothelial cells; COL4A3, Collagen Type IV Alpha 3 Chain; DMSO, Dimethylsulfoxide; DSO, Descemet Stripping Only; ECL, Enhanced chemiluminescence; EGFR, Epidermal growth factor receptor; EK, Endothelial keratoplasty; FBS, Fetal bovine serum; FECD, Fuchs endothelial corneal dystrophy; FNC, Fibronectin and collagen; GAPDH, glyceraldehyde-3-phosphate dehydrogenase; GSK3α, Glycogen synthase kinase 3 alpha; HRP, Horseradish peroxidase; ICC, Immunocytochemistry; LDV, Low dead volume; LIMK1, LIM domain kinase 1; LIMK2, LIM domain kinase 2; LVB4G12, Lentiviral transduced immortalized corneal endothelial cell line; MKK4, Mitogen-Activated Protein Kinase 4; MLCK4, Myosin light chain kinase 4; MOI, Multiplicity of infection; MRCK, Myotonic dystrophy-related Cdc42-binding kinase; MRCKα, Myotonic dystrophy-related Cdc42-binding kinases α; MRCKβ, Myotonic dystrophy-related Cdc42-binding kinases β; MSK1, Mitogen- and stress-activated kinase 1; MTS, MTS tetrazolium salt 3-(4,5-dimethylthiazol-2-yl)-5-(3-carboxymethoxyphenyl)-2,4-sulfophenyl-2H-tetrazolium; Na⁺/K⁺ATPase, Sodium potassium adenosine triphosphatase; OrBITS, Organoid Brightfield Identification-based Therapy Screening; P16, Cyclin-dependent kinase inhibitor 2A; P38α, P38 mitogen-activated protein kinase alpha; PBS, phosphate-buffered saline; PKA, Protein kinase A; PKAcα, Protein kinase A catalytic subunit; PKC, Protein kinase C; PKCα, Protein kinase C alpha; PKG, Protein kinase G; PKN, Protein kinase N1; PRDX6, Peroxiredoxin-6; RIPA, Radioimmunoprecipitation; ROCK1, Rho-associated coiled-coil containing protein kinase 1; ROCK2, Rho-associated coiled-coil containing protein kinase 2; ROCKi, Rho-associated coiled-coil containing kinase inhibitor; RT, Room temperature; SLCA11, Solute carrier family member 11; Src, Proto-oncogene tyrosine-protein kinase; TBS, Tris-Buffered Saline; ZO-1, Zonula occludens-1.

* Corresponding author at: Institute of Molecular and Translational Medicine, Faculty of Medicine and Dentistry, Palacky University Olomouc, Olomouc, Czech Republic.

E-mail addresses: hendrik.vercammen@uantwerpen.be (H. Vercammen), Bert.VandenBogerd@uantwerpen.be (B. Van den Bogerd).

<https://doi.org/10.1016/j.bioph.2024.116435>

Received 10 January 2024; Received in revised form 6 March 2024; Accepted 15 March 2024

Available online 20 March 2024

0753-3322/© 2024 Published by Elsevier Masson SAS. This is an open access article under the CC BY-NC-ND license (<http://creativecommons.org/licenses/by-nc-nd/4.0/>).

indicating possible cellular stress. In compared parameters, Chroman-1 at a concentration of 10 nM outperformed other ROCKi, requiring significantly 1000-fold lower effective concentration than established ROCKi Y-27632 and Fasudil. Altogether, this study underscores the potential of repurposing ROCKi for treating corneal endothelial dysfunctions, offering a viable alternative to conventional grafting methods, and highlights Chroman-1 as a promising candidate structure for hit-to-lead development.

1. Introduction

The corneal endothelium constitutes the innermost layer of the cornea, often metaphorically described as the transparent 'window' through which our body observes its exterior environment. Its integrity is crucial for maintaining corneal transparency [1]. In 2019, corneal opacification, a condition when the cornea becomes opaque and thus negatively affects vision, emerged as a leading cause of blindness, affecting around 4.2 million individuals globally [2]. The diseases causing corneal opacification are primarily Fuchs endothelial corneal dystrophy (FECD), bullous keratopathy, posterior polymorphous dystrophy, congenital hereditary endothelial dystrophy, and iridocorneal endothelial syndrome [3]. FECD stands out as the most common condition, exhibiting a prevalence of 3.8–11% in individuals over 40 years old and being the foremost reason for corneal transplantation worldwide [4].

The preservation of corneal transparency depends significantly upon the optimal functioning of the corneal endothelial cells (CEnCs) [5,6]. These cells regulate corneal hydration levels via a dynamic interplay of leaky tight junctions and active ion pumps represented by the expression of key proteins zonula occludens-1 (ZO-1) and Na⁺/K⁺ ATPase, respectively. Current consensus indicates a significant lack of regenerative capacity in the post-mitotic state of CEnCs, which are maintained in G0/G1 phase of the cell cycle [7,8]. Damage or dysfunction of these cells disrupts corneal hydration, disturbing the meticulously organized collagen lamellae within the stroma. Elevated hydration levels cause a misalignment of these lamellae, culminating in light scattering and corneal opacity, ultimately resulting in visual impairment and potentially corneal blindness [9]. Hence, the development of treatments that enhance the patient's own cell regeneration capacity is highly pertinent in exploring novel and alternative methods to address corneal endothelial decompensation. This is especially crucial due to the widespread shortage of donor tissue for posterior keratoplasty, a surgical procedure replacing damaged or dysfunctional endothelial cells on the cornea's inner layer [10–12]. An alternative approach is to enhance the regenerative capacity by leveraging the existing drugs already approved for another condition with an established safety profile, also known as drug repurposing, repositioning, or re-tasking [13–15]. Recently, the strategy of drug repurposing has gained significant traction; as much as 33% of newly approved drugs correspond to repurposed ones, which now account for approximately 25% of the annual pharma industry revenue [14,16]. Such compounds are also Rho/Rho-associated coiled-coil containing kinase (ROCK) inhibitors (ROCKi), as four of them are already FDA-approved (Netarsudil, Fasudil, Ripasudil and Belumosudil) [17–19].

ROCKi comprise a class of compounds that have gained interest across diverse research fields, including cardiology, neurology, and osteology, for their regenerative effects on tissue [20–22]. ROCKi have found applications in glaucoma and ocular hypertension, attributed to their impact on axonal regeneration and actin dynamics of trabecular meshwork cells, respectively [23]. Despite the fact that the FDA has yet to approve a defined standard ROCKi treatment to catalyze corneal endothelial regeneration, ROCKi have proven their potential within corneal endothelial tissue regeneration over several years. A recent phase 1 double-masked and randomized clinical trial tested compound Y-27632, the most extensively studied ROCKi in preclinical research, as a supplement for endothelial cell therapy to address corneal endothelial dysfunction (NCT05309135) [24]. Hence, in the field of corneal

endothelial regeneration, ROCKi appear to present a promising therapeutic approach, given that the ROCKi target key molecules of signaling pathways associated with regeneration, which consists mainly of proliferation and migration [25]. However, the exact mechanisms of action and pharmacokinetics have not been fully elucidated, thereby hampering the translation into the clinic [25–27]. Thus, the established pharmacological profile of these regenerative small molecules in different research areas can be utilized for the purpose of corneal endothelial regeneration (Table 1).

Harnessing the ROCKi capabilities to enhance the proliferation and migration potential of CEnCs could provide a vital step to counteract corneal endothelial dysfunctions. Therefore, applying the principle of drug repurposing for corneal endothelial regeneration on the self-assembled ROCKi library (Table 1), is a rational approach to discovering regenerative drugs for patients suffering from corneal endothelial dysfunctions.

Live cell imaging emerges as a pivotal player in the future of pharmaceutical drug discovery. This technique warrants the delivery of kinetic, image-based data that can reveal both the qualitative and quantitative aspects of cellular drug responses, defined as phenomics [28,29]. Compared to end-point analysis (e.g., resazurin-based assays), time-lapse live imaging microscopy offers a platform for drug screenings that dynamically captures parameters of interest [30]. At the same time, integrating machine learning techniques augments the ability to identify measurable parameters and generate cell type-specific phenotypic measurements [31]. As opposed to conventional analysis methods that directly compare single parameters, machine learning techniques facilitate customizable high throughput analysis [31,32]. In this aspect, OrBITS, an image and data analysis platform, provides a platform to quantify large image-based datasets in a high throughput manner [33].

Here, we report the repurposing of ROCKi to stimulate the growth of corneal endothelial cells, offering a potential pharmacological alternative to corneal endothelial transplantation. Our objective is to explore how live cell imaging techniques, combined with metabolic and protein-based assays, will serve as the pillars of the described screening pipeline. This research aims to create a comprehensive and effective approach for screening small molecules specifically for corneal endothelial regeneration.

2. Materials and methods

2.1. ROCKi library

The compounds for a self-assembled ROCKi library were purchased from MedChemExpress (Monmouth Junction, USA), containing 100 µL of 10 mM stock concentrations of fifteen ROCKi dissolved in dimethyl sulfoxide (DMSO), differing in potency (EC₅₀ and K_i values) and target selectivity (Table 1). These inhibitors have been recognized for their applications in numerous research domains, including cancer, metabolic disorders, and cardiovascular diseases. Two different stock solutions were prepared (10 mM and 0.1 mM) and transferred into a 384 low dead volume (LDV) plate (Labcyte, CA, USA), compatible with the Echo 555 liquid handler (Labcyte, CA, USA) used for drug dispensing. DMSO (Labcyte, CA, USA) and 2 µM staurosporine (SelleckChem, PA, USA) were included in the LDV plate as the control conditions.

Table 1
Self-assembled ROCK inhibitor library.

ROCK inhibitor	Research area	IC ₅₀ value	K _i value	Alternative target proteins
Fasudil CID: 3547	Cancer and cardiology	ROCK2: 0.158 μM	ROCK1: 0.33 μM	PKA, PKC and PKG
Ripasudil CID: 9863672	Neurology	ROCK1: 51 nM ROCK2: 19 nM	/	PKC, CaMKIIa and PKAcA
RKI-1447 CID: 60138149	Cancer	ROCK1: 14.5 nM ROCK2: 6.2 nM	/	/
Thiazovivin CID: 1269048	Cancer	Non-specific for ROCK1 and ROCK2: 0.5 μM	/	/
Y-27632 CID: 448042	Cancer	/	ROCK1: 220 nM ROCK2: 300 nM	PKN, PKA, PKCα and Citron kinase
Y-33075 CID: 9810884	Cancer	Non-specific for ROCK1 and ROCK2: 3.6 nM	/	PKC and CaMKII
ZINC00881524 CID: 1138914	Cancer	/	/	/
Belumosudil CID: 11950170	Immunology	ROCK1: 24 μM ROCK2: 105 μM	/	/
ROCK inhibitor-2 CID: 51003130	Immunology and cardiology	ROCK1: 17 nM ROCK2: 2 nM	/	/
BDP5290 CID: 85325326	Cancer	ROCK1: 5 nM ROCK2: 50 nM	/	MRCKα and MRCKβ
LX7101 CID: 56962369	Cancer	ROCK2: 10 nM	/	PKA, Akt1, LIMK1 and LIMK2
SR-3677 CID: 25093235	Cancer	ROCK2: 3 nM	/	/
Chroman 1 CID: 66577033	Cardiology	ROCK1: 52 pM ROCK2: 1 pM	/	MRCK
SAR407899 CID: 15604510	Metabolic diseases	ROCK2: 135 nM	/	PKC and MSK1
H-1152 CID: 448043	Neurology	ROCK2: 12 nM	/	CaMKII, PKG, AuroraA, PKA, Src, Abl, PKC, MKK4, MLCK, EGFR, GSK3α, AMPK and P38α

Table 1 contains ROCKi, used in various other research fields and differing in selectivity to its target proteins and potency (IC₅₀ values or K_i values provided by the vendor). The alternative target proteins (other than ROCK1 and ROCK2) are described in the last column. CID represents the compound identification number.

2.2. Cell culture

An immortalized corneal endothelial cell line (B4G12) was purchased from the Deutsche Sammlung von Mikroorganismen und Zellkulturen Institute (Braunschweig, Germany). B4G12 cells were cultured in human endothelial serum-free medium (ThermoFisher Scientific, MA, USA) supplemented with 10 ng/mL basic fibroblast growth factor

(bFGF, Life technologies, California, USA). The culture flasks and 384 well plates were coated with fibronectin and collagen mix (FnC mix, Athena Enzyme systems, Baltimore, USA) to facilitate the attachment of B4G12 cells. The B4G12 cells were sub-cultured every three days for a minimum of two weeks prior to the start of the experiments. B4G12 cell line was transduced with lentiviral particles (rLV.EF1.mCherry-Nuc-9, Takara, Göteborg, Sweden) at an MOI of 40 and 5 μg/mL of Polybrene (Sigma-Aldrich, MA, USA) resulting in a LVB4G12 cell line with red fluorescence nuclei. Post-transduction, LVB4G12 cells were sorted using FACS Aria II SORP flow cytometer based on red fluorescence signal (excitation 587, emission 610) to obtain cells with strong red nuclear signal. After sorting, cells were selected using puromycin (Gibco, ThermoFisher Scientific, MA, USA) at a working concentration of 1 μg/mL. Both B4G12 and LVB4G12 cells were passaged using TrypLE (Gibco, ThermoFisher Scientific, MA, USA), and expanded in a T-180 flask, kept at 37 °C in a 5% CO₂ environment. In preparation for drug screening assays, 384 well plates (PerkinElmer cell carrier black clear, MA, USA) were coated with the FnC mix using a MultidropCombi microplate dispenser (Thermo Fisher Scientific, MA, USA), dispensing 4 μL FnC coating/well, followed by plate centrifugation for one minute at 200 x g to ensure even distribution of the coating. The Cells were passaged and seeded at a density of 2.25 × 10³ cells per well in a 384 well plate, in human endothelial serum-free medium using MultidropCombi microplate dispenser, and incubated overnight prior to ROCKi treatment. In general, cell passage numbers exceeding twenty were too high and, therefore, not utilized for experimental testing. For each biological replicate, the cell passage numbers varied between eight and fourteen.

2.3. Validation of DMSO limit

To identify the highest suitable DMSO concentration for ROCKi treatments without affecting the growth and motility of B4G12 cells, D300e digital dispenser (Tecan, Männedorf, Swiss) was employed to test twelve logarithmically distributed DMSO concentrations ranging from 4.76% to 0.04%. B4G12 cells at a density of 5.50 × 10⁴ were seeded into 96 well Imagelock plates (Essen Bioscience, Hertfordshire, United Kingdom), in seven technical replicates for each concentration, and scratched as described in [Section 2.6 \[34\]](#). As a negative control, 2 μM staurosporine was included. Post-treatment, the cells were imaged using the IncuCyte® ZOOM device (Sartorius, Göttingen, Germany) every four hours for five days. The IncuCyte® ZOOM 2018 software module (Sartorius, Göttingen, Germany) was used for data analysis and for the masking process to quantify relative scratch wound closure percentages from the images. The scratch wound closure percentage was utilized to generate a dose-response curve (log inhibitor vs. response curve) for the different DMSO conditions.

2.4. Cell viability (MTS assay)

The MTS assay, a non-imaging-based colorimetric method, was used to quantify the cell viability, thereby investigating the cytotoxicity of fifteen ROCKi on LVB4G12 cells. The MTS assay was conducted with a CellTiter 96 Aqueous One Solution Cell Proliferation Assay (Promega, WI, USA), according to the manufacturer's instructions. LVB4G12 cells were seeded in FnC-coated 384 well clear plates (TPP, Trasadingen, Switzerland) at 2.25 × 10³ cells per well and incubated for 24 hours. Next, ROCKi were added, and MTS assay was performed five days post-treatment. After incubation with MTS solution for 3 hours at 37 °C and 5% CO₂, the absorbance was measured at 490 nm using the Envision microplate reader (Perkin Elmer, MA, USA).

2.5. Proliferation assay

Live cell imaging was used for the endpoint and kinetic analysis of the ROCKi. LVB4G12 cells were seeded in FnC-coated 384 well plates (Cell carrier black with clear bottom, PerkinElmer, MA, USA) at 2.25 ×

10^3 cells per well and incubated for 24 hours. Echo 555 liquid handler (Labcyte, CA, USA) was used to dispense ten distinct concentrations of each compound, ranging from 50 μM to 5 nM. Yokogawa CV8000 live cell imager (Yokogawa Electric Corporation, Musashino, Japan) with a 10x dry lens captured four images per well (reflecting the whole well in a 384 well plate setup) each day over a five-day measuring period. Brightfield images and red fluorescent images (excitation 587 nm, emission 610 nm), were used as raw data in the masking procedure, which extracts numerical data out of the images to quantify cell growth. In this regard, the OrBITS platform was used as an automated data processing tool where the images were processed based on a deep learning algorithm to extract accurate cell counts out of the red fluorescent image, representing the nuclei of the LVB4G12 cells [33]. The calculation of the area under the curve (AUC) values for quantification of growth trajectory was performed only for the ROCKi that were identified with significantly elevated cell count numbers relative to the control (DMSO). The AUC units (cells x hours) summarize the entire trajectory of growth.

2.6. Scratch wound assay

To assess the wound healing potential of B4G12 cells post-ROCKi compound treatment of the nine selected ROCKi conditions, a scratch wound assay was performed [34]. B4G12 cells were seeded at a density of 5.50×10^4 cells/well in 100 μL in 96 well Imagelock plates (Essen Bioscience, Hertfordshire, UK), pre-coated with FnC coating mix. These plates were incubated overnight to allow cells to attach and create a fully confluent monolayer. Subsequently, the Incucyte woundmaker tool (Essen Bioscience, Hertfordshire, UK) was used to introduce uniform linear scratches ranging between 700 and 800 μm in width into the confluent monolayer of B4G12 cells [35]. Immediately post-scratching, the cells were washed twice using 100 μL PBS solution to remove any cellular debris within the wound. Following this, each well was inspected under an EVOS FL digital inverted microscope (Life Technologies, California, USA) to validate the scratches. The ROCKi compounds were then administered with the Tecan D300e drug dispenser (Tecan, Männedorf, Switzerland). Subsequently, the 96 well plates were transferred to Incucyte ZOOM's live cell imaging system (Sartorius, Göttingen, Germany) and imaged at four-hour intervals over six days. The phase contrast was acquired with 10x objective lens (Nikon, Tokyo, Japan), with image acquisition set to one image/well. Images collected were processed through the Incucyte ZOOM 2018 software (Sartorius, Göttingen, Duitsland). Five representative images were segmented using a manually adjustable masking procedure, refined by parameters like area, eccentricity, and mask size to improve label-free mask fitting and eliminate artifacts. The refined process was then applied to all images, and phase object confluence (%) was extracted and plotted over time. The calculation of AUC values for quantification of entire wound closure trajectory was performed. The AUC units ((cells/ μm^2) x hours) summarize the whole trajectory of the wound closure in scratch wound assay, implying the number of cells per μm^2 after 120 hours of treatment.

2.7. Image quantification

The image data of the proliferation assay was quantified utilizing an artificial intelligence (AI)-powered analysis software, OrBITS [33]. Specifically, OrBITS employs dynamic object detection and classification networks, known as semantic segmentation convolutional neural networks for data processing. The data from kinetic analysis and end-point measurements, which include images identifying nuclei and cells, were then converted into quantifiable metrics. Additionally, the Incucyte ZOOM software platform, with its integrated machine-learning technology, was employed to extract and quantify relative wound density percentage and the wound closure rate expressed as AUC values which resembles the complete wound healing trajectory.

2.8. Immunocytochemistry (ICC)

B4G12 cells were seeded into 96 well plate (PhenoPlate, Perkin Elmer, MA, USA) at concentration 1×10^4 cells/well. Nine selected ROCKi were added to cells and incubated for four days. Fixation of the cells with 4% paraformaldehyde was performed for 30 minutes at room temperature (RT). Afterwards, the plates were washed four times with PBS and incubated with 100 μL of permeabilization solution (Triton X 0.25% in PBS) for ten minutes. After permeabilization, cells were washed twice with PBS. Next, 100 μL of blocking solution (5% FBS in PBS with 0,05% Tween 20) was added for 1.5 hours at RT. Plates were incubated with primary antibodies overnight at 4 °C. The dilutions for the primary antibodies were: 1:500 for Na^+/K^+ ATPase (Abcam; ab76020, Cambridge, UK) and 1:200 for Zonula occludens-1 (ZO-1) (Abcam; ab221547, Cambridge, UK). The next day, the plates were washed with wash solution (PBS with 0,05% Tween 20) and incubated with the secondary antibodies (goat anti-mouse IgG, Invitrogen, A21052; goat anti-rabbit IgG, Invitrogen, A11034, MA, USA) for one hour at a dilution of 1:250 RT. Next, the plates were washed three times with wash solution and incubated with 10 $\mu\text{g}/\text{mL}$ Hoechst33342 in PBS for 15 min at RT for nuclei staining. Brightfield, green fluorescent signal (excitation 631 nm; emission 650 nm) and blue fluorescent signal (excitation 352 nm; emission 454 nm) were captured by a $20 \times$ PH Long W.D. or 60x objective of the Yokogawa CV8000 live cell imager (Yokogawa Electric Corporation, Musashino, Japan). The data was postprocessed and analyzed by Columbus software version 2.7.1 (PerkinElmer, MA, USA).

2.9. Western Blot

The B4G12 cell line was seeded in FnC-coated T25 flasks at the seeding density of 1.25×10^6 cells. Following a 24-hour incubation period, nine ROCKi were introduced, and cells were incubated for an additional 72 hours. Subsequently, the cells were harvested, centrifuged three times at 100 x g for five minutes at 4 °C, each time washed with PBS. Cells were lysed in ice-cold RIPA buffer (150 μM NaCl, 1% NP-40, 0.5% sodium deoxycholate, 0.1% SDS, 50 μM Tris-HCl at pH 8.0, and 1 μM EDTA) for 30 minutes, followed by sonication for one minute at 4 °C in ultrasonic water bath and centrifugation at 14,000 x g for 15 minutes at 4 °C. Protein concentrations were determined using a BCA protein assay (ThermoFisher Scientific, MA, USA; REF23208). Upon the addition of Laemmli buffer, the protein samples were incubated at 70 °C for 10 minutes. Equal protein concentration of samples was fractionated using 12% SDS-PAGE and transferred onto nitrocellulose membranes using a semi-dry blotting method (Trans-Blot Turbo Transfer System; Bio-Rad Laboratories, Inc., CA, USA). The membranes were then blocked with 5% BSA (150 mM NaCl, 50 mM Tris-HCl at pH 7.6) containing 0.1% Tween-20 for an hour at RT, followed by overnight incubation at 4 °C with the primary antibodies at dilution ratio of 1:1000 (ZO-1, 51–9000, ThermoFisher Scientific, MA, USA; Cyclin E1, HE12, Cell Signaling Technology, MA, USA; CDK2, 2546 T, Cell Signaling Technology, MA, USA; p16, 1/1000, p-0968, Sigma Aldrich, MI, USA). The next day, the membranes were rinsed in TBS with 0.1% Tween-20 and incubated at RT for one hour with HRP-conjugated secondary antibodies (Cell Signaling Technology, MA, USA). Chemiluminescence was detected using ECL (enhanced chemiluminescence) substrate and ChemiDoc MP Imaging System (Bio-Rad Laboratories, Inc., CA, USA). Images were analyzed by Image Lab software v6.1 (Bio-Rad Laboratories, Inc., CA, USA).

2.10. Statistics

All data was tested for normality. Normally distributed data was used to generate a quantile-quantile plot to show the distribution of the data against the expected normal distribution. For all normal distributed data a one-way ANOVA analysis was performed (multiple comparisons). For

all not normal distributed data, the Kruskal-Wallis test with multiple comparisons and the non-parametric t-test was used. In all tests, a p-value equal to or less than 0.05 was considered to be significant.

3. Results

3.1. Establishment of the DMSO limit for corneal endothelial cells

The ROCKi compound library is soluble in DMSO. However, the DMSO toxicity had not been evaluated for B4G12 cell line. In this regard, we tested via scratch wound analysis a broad range of DMSO concentrations, ranging from 4.76% to 0.04% in a logarithmic distribution, alongside with staurosporine at a concentration of 2 μM as negative control. We observed an increase in relative wound density of 75% after five days, when treated with DMSO concentrations lower than 1.28% indicated in purple (Fig. 1A), reflecting regular wound closure. On the contrary, DMSO concentrations 1.99% - 4.76%, and 2 μM staurosporine exerted a toxic effect in the B4G12 cell line, limiting wound closure to a maximum of 50% after five days. In particular, 0.52% DMSO, similar to the DMSO concentration (0.5%) in the highest concentration of dissolved ROCKi (50 μM) intended for further screening, facilitated relative wound closure of more than 80%, hence not affecting the motility and growth rate of B4G12. The observations were further supported by a dose-response curve, with LogIC_{50} for DMSO equal to 2.033% (Fig. 1B). Thus, 0.5% DMSO was established as a non-toxic solvent limit, further used in the subsequent assays.

3.2. Assessment of ROCKi cytotoxicity

We performed MTS assay to investigate the potential cytotoxicity of ROCKi library in a 10-point concentration-response format (Fig. 2). Normalization to the DMSO control (baseline) was adopted owing to the absence of an accepted standard positive control to stimulate B4G12 cell growth. Staurosporine was incorporated as a negative control to characterize cytotoxicity and DMSO as a vehicle, facilitating discrimination between toxic and non-toxic ROCKi conditions. Concentrations of ROCKi identified as toxic are depicted in red with white asterisks, namely BDP5290 (50 μM ; 25 μM), Belumosudil (50 μM ; 25 μM ; 10 μM ; 5 μM), LX7101 (50 μM ; 25 μM), H-1152 (50 μM), RKI-1447 (50 μM), and ZINC00881524 (50 μM). Ripasudil, ROCKi-2, Y-33075, Y-27632, SAR407899, SR-3677, Thiazovivin, Fasudil and Chroman-1 in a

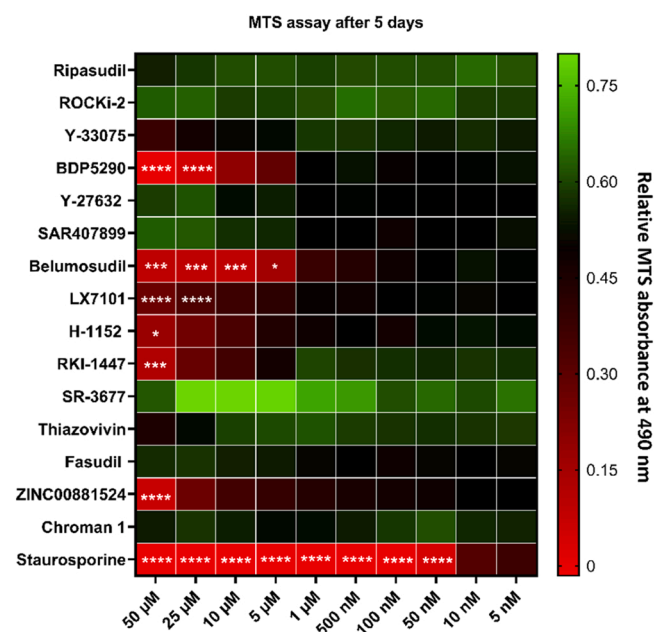


Fig. 2. Viability of B4G12 cells after ROCKi treatment. (A) Fifteen different ROCKi were tested in ten concentrations ranging from 50 μM to 5 nM. The heatmap consists of relative absorbance values (baselined with DMSO control condition) resembling the metabolic activity of the B4G12 cells measured after five days. A red color with asterisks represents the significant toxic condition. The different ROCKi conditions were statically compared via a one-way ANOVA (multiple comparisons), indicated by a p-value of less than 0.05 (* $p < 0.05$; ** $p < 0.005$; *** $p < 0.0005$; **** $p < 0.0001$). All experiments were done in three independent biological replicates ($n=3$).

concentration range from 50 μM to 5 nM did not hinder metabolic function of B4G12 compared to the control (0.5% DMSO). Of note, we observed that BDP5290 (50 μM ; 25 μM), LX7101 (50 μM ; 25 μM) and ZINC00881524 (50 μM) displayed a similar significant toxicity profile compared to 2 μM of staurosporine. Therefore, these compounds can be considered as the most cytotoxic ROCKi from the ROCKi library.

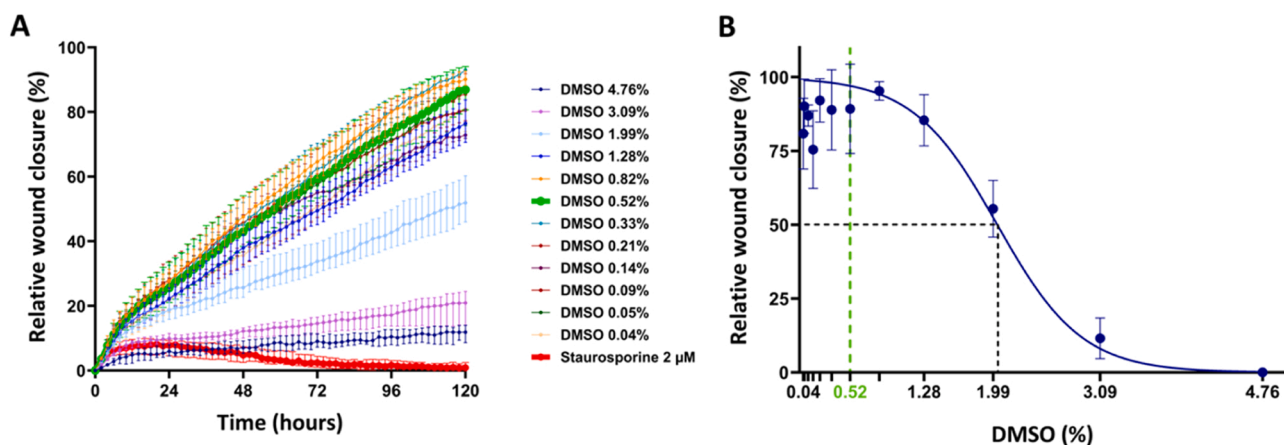


Fig. 1. Detection of DMSO limit via scratch wound analysis. (A) Twelve different DMSO concentration levels between 4.76% and 0.04% were tested to find the highest suitable DMSO limit. Data is represented in the figures as median \pm 95% confidence interval. The graph displays the relative scratch wound closure (%) of the different DMSO conditions over five days to quantify cell growth within the wound. 0.52% DMSO, equal to DMSO content in 50 μM ROCKi concentration, is shown via the bold green line. The staurosporine 2 μM condition, as the negative control, is displayed by the red line. (B) Dose-response curve of DMSO. The relative scratch wound closure (%) after five days is plotted against the different DMSO %. The LogIC_{50} value of DMSO ($\text{LogIC}_{50} = 2.033\%$), is indicated by the black dashed lines. The green dashed line indicates DMSO concentration not effecting B4G12 cell growth and motility. All experiments were done in three independent biological replicates ($n=3$).

3.3. ROCKi boost corneal endothelial cell growth

To evaluate the effect of ROCKi on corneal endothelial cell growth, we employed an image-based proliferation assay. Staurosporine (2 μM) was used as a negative control, representing a cytotoxic condition with an average cell count of 158 cells ± 42 cells, comprising dead cells and cellular debris. A concentration of 0.5% DMSO was used as the basal control and yielded a mean cell count of 779 ± 168 cells. The DMSO control was used as the basal growth control due to the lack of a golden standard positive control that stimulates B4G12 cell growth. End-point analysis was performed after five days to distinguish ROCKi with a proliferative effect from non-responders, cytostatic or cytotoxic ROCKi (Fig. 3A). The positive hit threshold was defined as exceeding the DMSO control condition by 3 SD (average cell count/field >1283 cells), indicated in orange. In this regard, several ROCKi conditions were identified with significantly elevated cell count numbers relative to the basal control in various concentration ranges. Namely, Ripasudil (5 μM), Y-27632 (50 μM; 25 μM), SAR407899 (50 μM; 25 μM; 10 μM), Thiazovivin (10 μM; 5 μM), Fasudil (50 μM; 25 μM; 10 μM) exceeded the hit threshold only with concentrations above 1 μM. On the other hand, ROCKi-2 (100 nM), Y-33075 (1 μM; 500 nM), SR-3677 (1 μM), and Chroman-1 (100 nM; 50 nM; 10 nM) enhanced cell growth at a concentration equal to or lower than 1 μM. The kinetic analysis of the ROCKi positive hits was performed over a period of five days (Fig. 3B). The growth over time of the LVB4G12 cells was measured and expressed as the AUC value. These results showed a significant increase in cell growth compared to the DMSO control over the entire measurement period.

3.4. ROCKi accelerate wound healing and closure

Nine ROCKi (Ripasudil, ROCKi-2, Y-33075, Y-27632, SAR407899, SR-3677, Thiazovivin, Fasudil, Chroman-1) from the image-based proliferation assay without any cytotoxic properties were further evaluated

via a scratch wound analysis. Here, we assessed the migration process of B4G12 cells, in addition to proliferation. Both processes, migration and proliferation occur during wound healing and serve therefore as a model for regeneration. The wound closure was expressed as relative wound closure percentage and was measured over time. Fig. 4A illustrates approximately 70% relative wound closure after five days for the DMSO control condition. Conversely, the wound treated with 2 μM staurosporine did not exhibit closure. Moreover, the wound area expanded over time due to cell death, resembling a cytotoxic response (data not shown). Every single ROCKi positive hit impacted B4G12 wound healing capability, as each experimental condition resulted in 70–90% relative wound closure after five days (Fig. 4A). To statistically substantiate this potential effect, the area under the curve value for each experimental condition was plotted and compared with the DMSO control condition. Most of the conditions demonstrated significantly faster wound closure relative to the DMSO control condition as indicated in Fig. 4B. However, the wound closure rate over time for SAR407899 50 μM, Fasudil 10 μM, Y-33075 0.5 μM, Chroman-1 0.05 μM treatment did not significantly deviate from the DMSO control condition.

3.5. Cell cycle regulators are not affected by selected ROCKi

We evaluated the expression of four proteins representing the fitness and cell cycle regulation of B4G12 cells after the treatment of selected ROCKi positive hits, namely, ZO-1, cyclin E1 (CCNE1), cyclin-dependent kinase 2 (CDK2), and cyclin-dependent kinase inhibitor 2 A (p16) by western blot analysis (Fig. 5A-B). The analysis of the key proteins involved in cell cycle progression (i.e., p16, CCNE1 and CDK2) is crucial to ensure that B4G12 cells, when treated with a ROCKi, maintain their ability to arrest cell cycle progression upon reaching a confluent monolayer. Selection of the following ROCKi: Y-27632, Chroman-1, Fasudil, ROCKi-2, SR-3677, Ripasudil, SAR407899, Thiazovivin, and Y-33075 with their concomitant optimal concentration was based on the results from previous screening assays, including MTS assay, image-

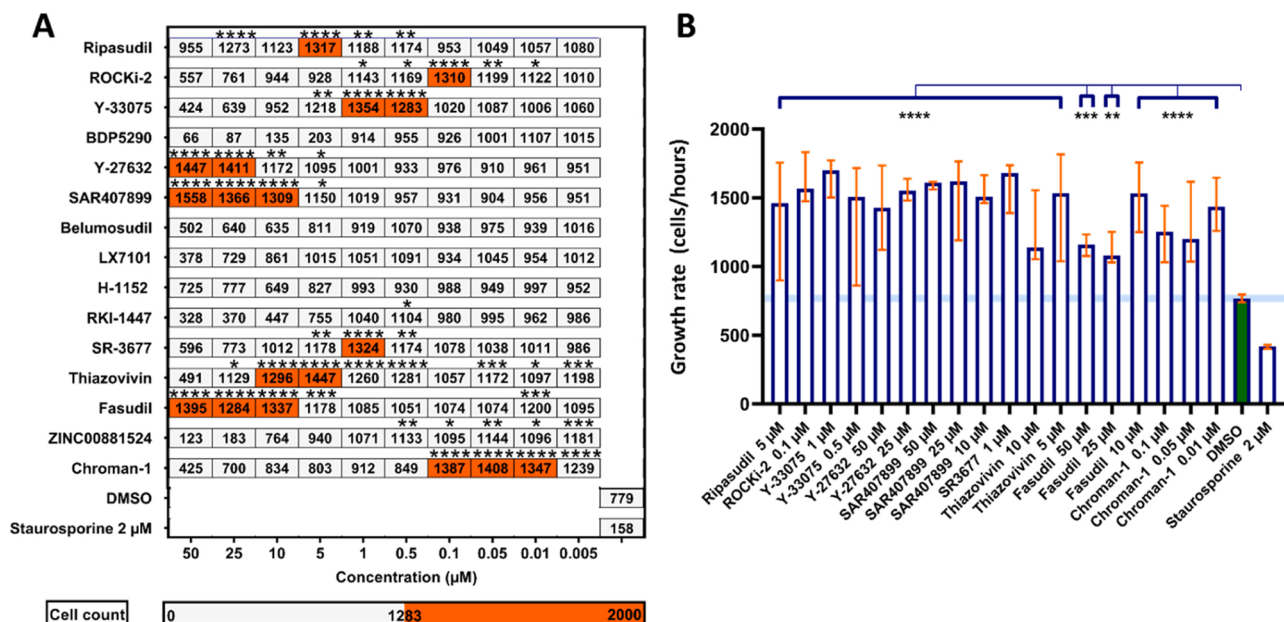


Fig. 3. Image-based proliferation assay of LVB4G12 cells after ROCKi treatment. (A) An average cell count of LVB4G12 cells five days post treatment with fifteen different ROCKi. The cell count map displays ten different concentrations of ROCKi, ranging from 50 μM to 5 nM. The cell counts are represented as a mean value/field in the well. The counts, highlighted in orange, represent ROCKi that exceed the basal control condition by 3 SD. One way ANOVA (multiple comparisons) test was performed. A p-value less than 0.05 was considered to be significant; *p<0.05; **p<0.005; ***p<0.0005; ****p<0.0001. (B) The area under the curve of the proliferation trajectories post-ROCKi treatment. The AUC value (cells x hours) encapsulates the five-day growth profile displayed in a bar-chart, represented by the median values within a 95% confidence interval. A non-parametric Kruskal-Wallis test was performed between the AUC values of ROCKi and AUC values of the DMSO basal control. A p-value of less than 0.05, was considered to be significant: **p<0.005; ***p<0.0005; ****p<0.0001. The blue-shaded region marks the area bounded by the lower and upper 95% confidence limits of the DMSO control. All experiments were done in three independent biological replicates (n=3).

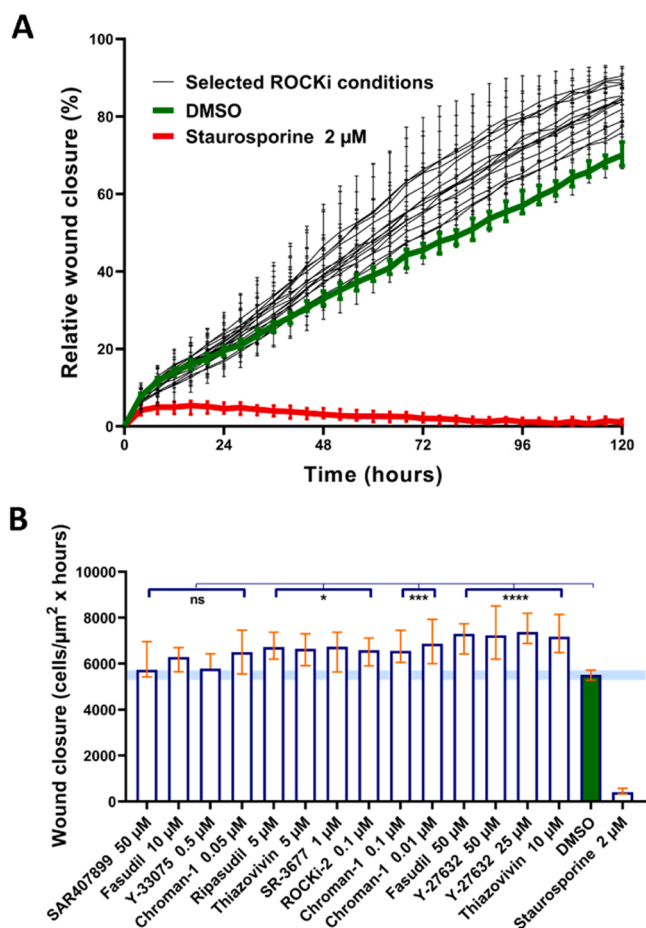


Fig. 4. Scratch wound analysis of B4G12 cells after ROCKi treatment. (A) Relative wound closure (%) over time of the ROCKi positive hits measured for five days after treatment. The identified hits are represented in black and the DMSO control condition is displayed in green. Staurosporine (2 μM), which is the negative control, is displayed in red. The graph represents the relative wound density expressed as median values with the 95% confidence interval over time. (B) Wound closure rate expressed as area under the curve (AUC) values for ROCKi positive hits compared to the DMSO control condition. The AUC values ((cells/ μm^2) x hours) represent the full wound healing trajectory of each condition after 120 hours. The data in the graph is represented as median values with 95% confidence interval. p values were calculated using a non-parametric Kruskal-Wallis test. p-value less than 0.05 was considered to be significant (* $p < 0.05$; *** $p < 0.0005$; **** $p < 0.0001$). All experiments were done in three independent biological replicates ($n=3$).

based proliferation assay, and scratch wound analysis. Outlier detection was systematically conducted on the data for all four proteins of interest, to ensure that the three independent biological repeats were representable to each other. The p16 protein, a cell cycle arrest marker, was confirmed to be present in all ROCKi treatment conditions with no statistically significant difference in relative p16 expression compared to the DMSO control. Similarly, for the two cell cycle progression markers, CDK2 and Cyclin E1, there was no observed significant difference compared to the untreated vehicle group. The results indicate that the cell cycle regulators behave similarly to the untreated control, suggesting no induced uncontrolled cell cycle. Furthermore, the relative ZO-1 expression treated by ROCKi-2, Ripasudil, Y-33075, SAR407899, Chroman-1, Fasudil and Thiazovivin showed a similar expression compared to the control group, indicating barrier integrity after treatment. Interestingly, the expression of ZO-1 in B4G12 cells treated with Y-27632 at a concentration of 25 μM was significantly lower compared to the control, as shown in Fig. 5A-B.

3.6. Chroman-1 exhibits no adverse effects on cellular tight junctions or Na^+/K^+ ATPase pump activity

We utilized immunocytochemistry analysis to assess the presence of two key corneal endothelial cell hallmark proteins in the plasma membrane. ZO-1, representing the functional intercellular tight junctions between B4G12 cells (Fig. 6), and Na^+/K^+ ATPase (Fig. 7), critical for maintaining the efflux of fluids from the stroma to the anterior chamber of the eye were examined [36–38]. Confocal microscopy detected the expression of ZO-1 across the nine ROCKi treatments. Nonetheless, substantial variations in ZO-1 expression were noted among the ROCKi conditions (Fig. 6A-B). Physiological ZO-1 expression is generally demonstrated by hexagonal-shaped cells (Fig. 6A), entirely delineated by ZO-1 [39,40]. On the contrary, treatments with SR-3677 1 μM , and Thiazovivin 10 μM depicted an aberrant ZO-1 expression (Fig. 6B), characterized by fragmented green signals. These conditions also indicated nuclear fragmentation and a high difference in cytoplasm size (i.e., polymegathism). Confocal microscopic examination of this negative condition validated a cytostatic state of cells, denoted by a weak ZO-1 signal and nuclear fragmentation. Nevertheless, it should be emphasized that some conditions, classified under physiological ZO-1 expression, had an aberrant-like profile, such as SAR407899 30 μM (Fig. 6A). A 20x magnified image captured polymorphic cells, while a 60x magnified image distinctly showed a B4G12 cell exhibiting a fragmented nucleus and enlarged cytoplasm. Moreover, Fig. 7 displays the Na^+/K^+ ATPase expression, which was observed across all experimental conditions, did not deviate from the control condition. Except for SR-3677 at a concentration of 1 μM condition, disclosed an aberrant Na^+/K^+ ATPase morphology.

4. Discussion

Currently, new emerging alternatives to conventional endothelial keratoplasty (EK) are being investigated to compensate for the scarcity in global corneal graft tissue [10–12,41–43]. Within the field of regenerative medicine, new therapeutic strategies aim to regenerate the corneal endothelium through pharmacological stimulation of the corneal endothelial wound healing process [44–46]. As part of the broader regenerative medicine field, we have proposed an innovative therapeutic approach aimed at catalyzing corneal endothelial renewal [9]. This alternative strategy offers a supplementary treatment option to the Descemet Stripping Only (DSO) surgical procedure. It addresses corneal endothelial dysfunction and reduces the reliance on donor tissue. Furthermore, a pharmacological strategy could be used as an add-on treatment in corneal endothelial surgery (i.e., EK) to increase the viability of the transplant. Moreover, in the development of novel cell therapies (i.e., ATMP) it could be used to accelerate the expansion of primary corneal endothelial cells *in vitro*, thereby drastically improving the translatability of basic ophthalmological research [9,47,48]. Our data indicates that ROCKi could be used as an alternative treatment to enhance the endogenous regeneration capacity of corneal endothelial cells [48].

In this study, DMSO was used to dissolve all analyzed ROCKi. Testing confirmed 1.28% DMSO as a tolerable cut-off value without affecting regular B4G12 cell physiology (Fig. 1) and to avoid precipitation of the compounds in high-concentration DMSO solutions [49]. Due to the lack of a golden standard positive control to stimulate B4G12 cell growth and motility, the 0.5% DMSO control concentration (equal to the highest amount of DMSO present in the 50 μM ROCKi treatment conditions) was used as the basal control condition when assessing the effects of ROCKi.

In a first-line screening (MTS assay and image-based proliferation assay), ROCKi were tested in concentration ranging from 50 μM to 5 nM. Two control conditions were included: a basal solvent DMSO control and a toxic, negative control (staurosporine 2 μM) [50]. We also formulated stringent hit selection criteria to identify compounds with a regenerative potential. Positive hits were selected based on a statistical threshold of

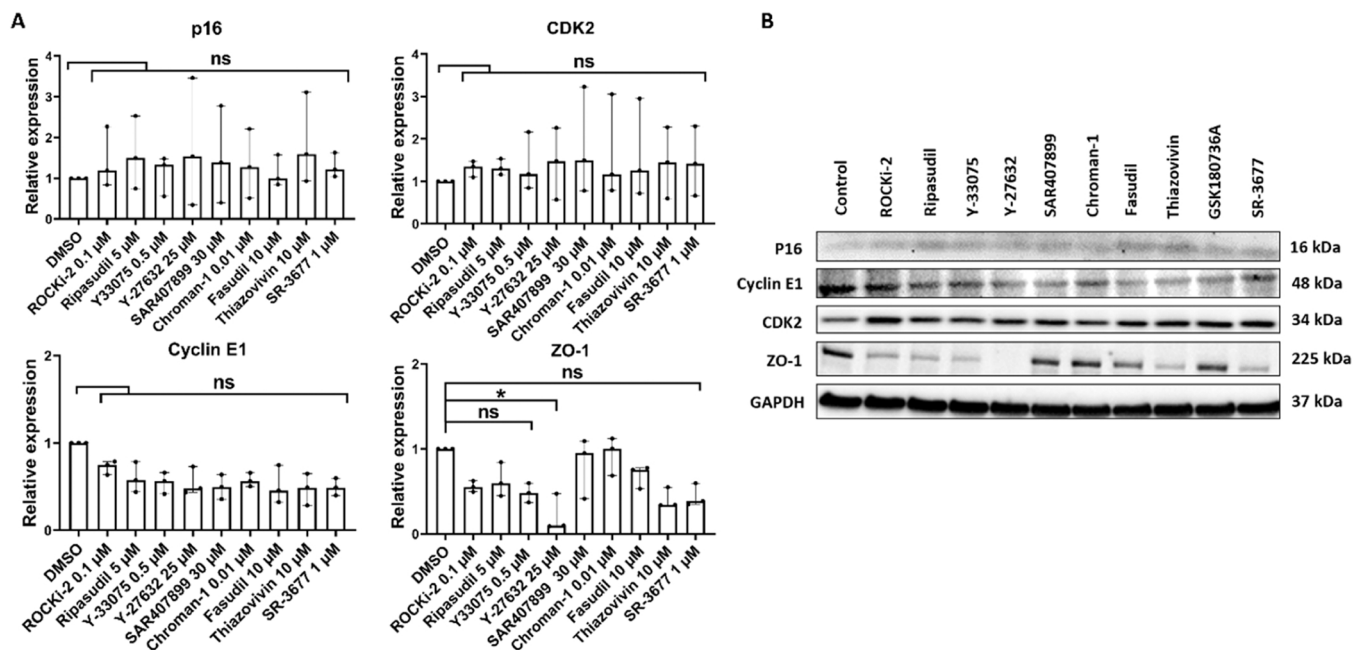


Fig. 5. Western blot analysis of B4G12 cells after ROCKi treatment. A) Relative protein expression of each experimental condition was normalized to GAPDH expression and statistically compared to the DMSO treated control by a non-parametric Kruskal-Wallis test for cyclin-dependent kinase inhibitor 2 A (p16), Cyclin E1 (CCNE1), Cyclin-dependent kinase (CDK2) and zonula occludens-1 (ZO-1). The data in the graphs is represented as median values with 95% confidence interval. p-value less than 0.05 was considered to be significant (* $p < 0.05$; ** $p < 0.005$; *** $p < 0.0005$; **** $p < 0.0001$). (B) Representative immunoblots. The GSK180736 A compound was analyzed on the same blot but was not part of the self-assembled ROCKi library analyzed in this manuscript. Therefore, the relative protein expression for GSK180736 A was not calculated. All experiments were done in three independent biological replicates ($n=3$).

the mean plus three standard deviations of the control condition, ensuring that identified hits had significant positive proliferation effects, which were further tested via scratch wound analysis [51,52]. The MTS assay is suggested to be more suitable for toxicity studies rather than efficiently highlighting differences among promising regenerative compounds [53,54]. Hence, we identified highly toxic ROCKi conditions via the MTS assay (Fig. 2), which were further confirmed as toxic via a phenomic screening (the image-based proliferation assay; Fig. 3), including: BDP5290 (50 μM; 25 μM), Belumosudil (50 μM-5 μM), H-1152 (50 μM), RKI-1447 (50 μM), and ZINC00881524 (50 μM). The combination of both techniques (metabolic activity and imaged-based cell count) was applied to reduce the false positive hit rate and narrow down the conditions of interest through this pipeline. Remarkably, ROCKi-2 at 50 μM exhibited a non-toxic metabolic activity (MTS assay), while the absolute cell count (image-based proliferation assay) was below the control condition suggesting an inadequate growth profile. This implicates that an increased metabolic activity is not directly correlated with stimulating cell growth, which emphasize the benefit of combining these two techniques [55]. A series of ROCKi in various effective concentrations that indicated a potential hit in the image-based proliferation assay include: Fasudil (50 μM-10 μM), Chroman-1 (100–10 nM), SAR407899 (50 μM-10 μM), Ripasudil (5 μM), Thiazovivin (10 μM- 5 μM), Y-33075 (1 μM-500 nM), ROCKi-2 (100 nM), Y-27632 (50 μM-25 μM), SR-3677 (1 μM). These ROCKi were subsequently tested in scratch wound analysis (Fig. 4), as both proliferation and migration are key to wound healing [50,54]. Based on the data collected from scratch wound analysis, SAR407899 50 μM, Fasudil 10 μM, Y-33075 500 nM, Chroman-1 50 nM were identified to exhibit no significant acceleration of wound healing compared with the DMSO control group (Fig. 4B), although a significant positive effect on the cell proliferation was observed during the image-based proliferation assay (Fig. 3). Notably, Fasudil exhibited also less pronounced growth trajectory, as showed in Fig. 3B, indicating a delayed biological effect.

ZO-1 and Na^+/K^+ ATPase are accepted among scientists as indicators of a functional CEnC phenotype [9,56]. However, appropriate markers

for corneal endothelial cells are still under debate. Recent studies have suggested additional markers such as SLCA11, ALCAM, PRDX6, and COL4A3 for corneal endothelial phenotype profiling [57]. We applied ICC analysis to examine the expression ZO-1 and Na^+/K^+ ATPase. Abnormal morphology of ZO-1 was observed in a number of B4G12 cells after ROCKi treatment, including SR-3677 1 μM and Thiazovivin 10 μM (Fig. 6B). The presence of enlarged, polynuclear cells might induced cellular stress or senescence, requiring further exploration using methods like the beta-galactosidase assay [58]. Na^+/K^+ ATPase physiological membrane expression was present in all the ROCKi conditions except for SR-3677 at 1 μM which shows an aberrant expression (Fig. 7). Protein expression analysis revealed a lower ZO-1 expression in Y-27632 at a concentration of 25 μM, suggesting a relative compromised barrier function of B4G12 cells compared to other ROCKi. The latter showed a similar ZO-1 expression compared to the untreated DMSO control. Interestingly, all ROCKi conditions formed a complete monolayer but the offset of the ZO-1 formation differs between the ROCKi because ICC analysis showed the presence of ZO-1 [59]. Furthermore, all ROCKi maintained expression of the p16 cell cycle arrest marker. Expression profiles of cyclin E1 and CDK2 showed no significant difference compared to the control, indicating a non-disturbed B4G12 cell cycle. The expression of p16, Cyclin E1 and CDK2 is crucial to ensure that B4G12 cells, when treated with a ROCKi, maintain their ability to arrest cell cycle progression upon reaching confluence [60,61]. However, interpreting the protein expression demands caution. For a broader understanding, future transcriptomic and kinome analysis of the up-regulated and downregulated pathways and kinase activity (i.e. ROCK 1 and/or ROCK 2) is required [62,63].

The results from the ROCKi screening highlighted several promising drug candidates exhibiting positive effects on cell growth and the corneal endothelial regeneration capacity, that have not been described in the literature yet (i.e. ROCKi-2, Chroman-1 and SAR407899). In particular, Chroman-1, exhibiting positive effect at 10 nM, emerged as a promising compound for future hit-to-lead optimization. In addition, Table 1 showed that Chroman-1 is a potent inhibitor of ROCK1 and

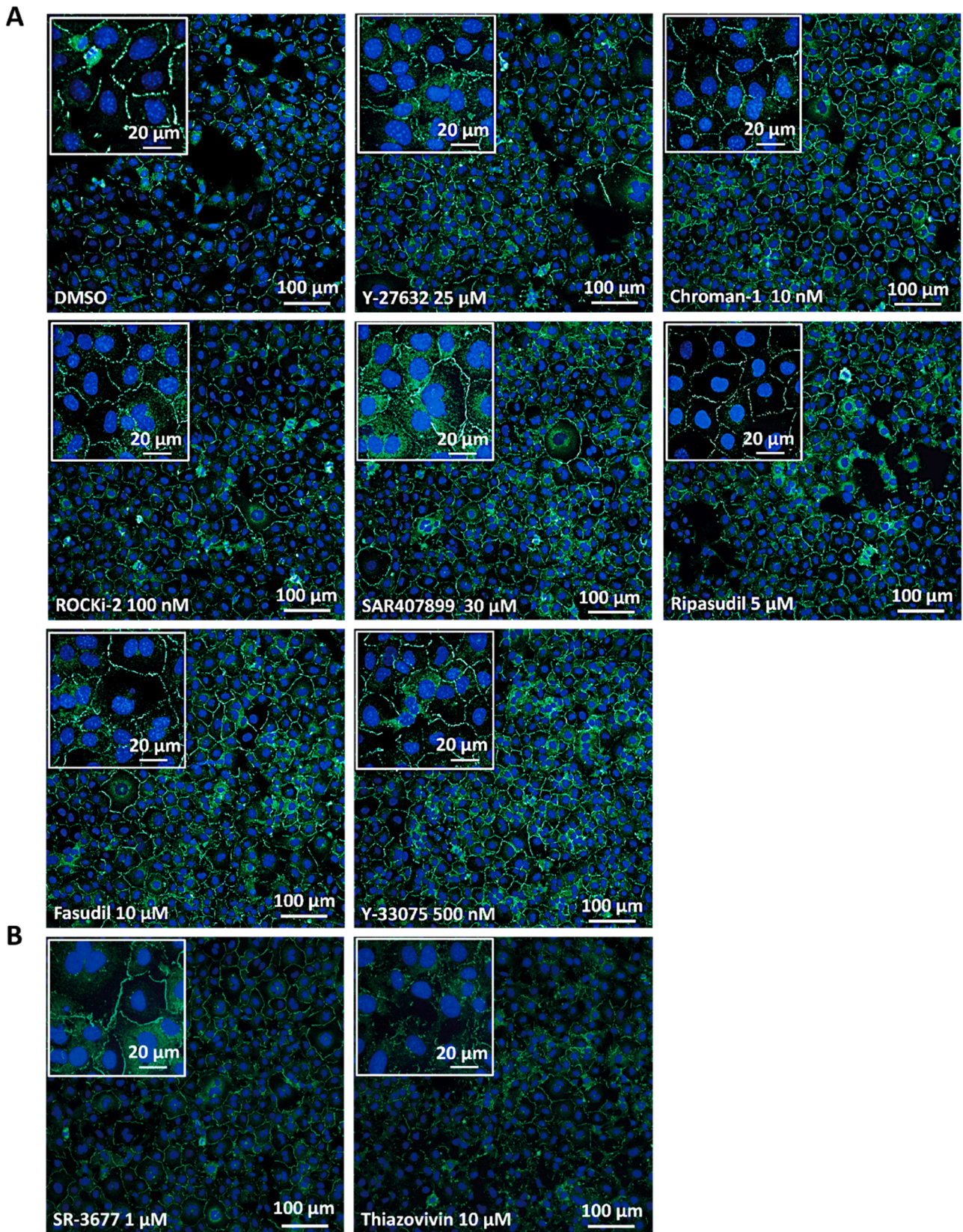


Fig. 6. Confocal images showing ZO-1 expression (green) of B4G12 cells after ROCKi treatment. (A) Physiological ZO-1 expression (green signal) after ROCKi treatment. (B) Aberrant ZO-1 expression after ROCKi treatment. DMSO control reflects normal ZO-1 expression. Nuclei were stained with Hoechst33342 dye (blue). Scale bar: 20 μm, 100 μm. All experiments were done in three independent biological replicates (n=3) and one representative image is shown.

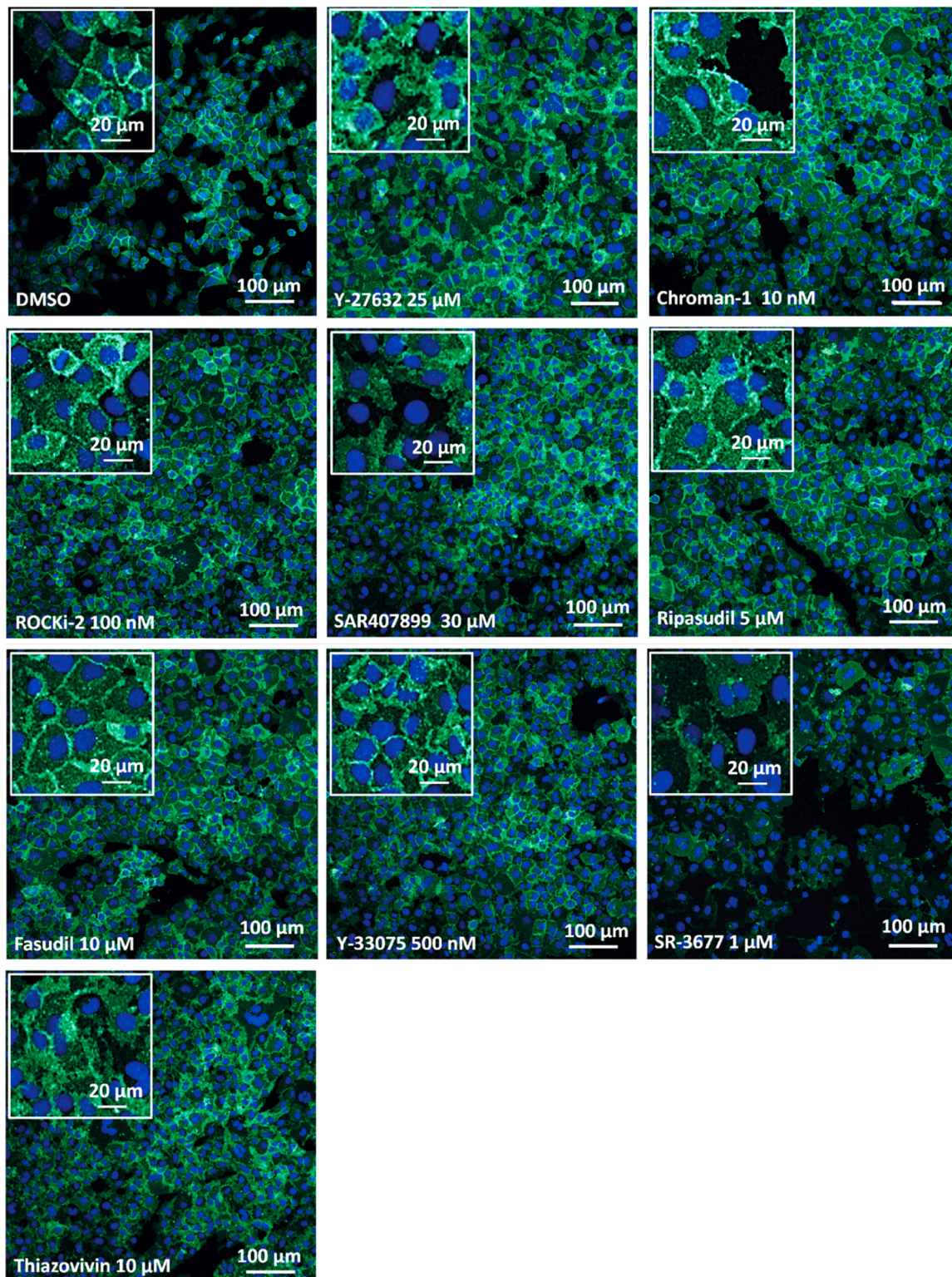


Fig. 7. Na^+/K^+ ATPase protein expression of B4G12 cells after ROCKi treatment. Na^+/K^+ ATPase staining (green signal) of B4G12 cells after ROCKi treatment. Nuclei were stained with Hoechst33342 dye (blue signal). The control treated with DMSO reflects the basal condition. Scale bar: 20 μm , 100 μm . All experiments were done in three independent biological replicates ($n=3$) and one representative image is shown.

ROCK2 with myotonic dystrophy-related Cdc42-binding kinases (MRCK) as an alternative target and mainly under investigation in the field of cardiology [64]. These findings underscore the regenerative potential of the ROCKi compound class, evidenced through *in vitro* screenings, in managing corneal endothelial dysfunction. Chroman-1 managed to compete and even exceed known effective ROCKi, such as

Y-27632 and Fasudil, with optimal concentrations up to 1000 folds lower, which can possibly lead to decreased off target and side effects [47]. However, signaling pathway and kinome analysis are required to completely understand how different ROCKi stimulate corneal endothelial regeneration and to pinpoint optimal conditions and dosage for their translational use [25,65]. Moreover, the integration of additional

multi-omics techniques such as metabolomics, proteomics, and lipidomics will be applied to discover both new targets and their associated biological effects, alongside identifying novel biomarkers.

5. Conclusion

The literature shows that Fasudil, Ripasudil, Thiazovivin, Y-33075, and Y-27632 positively impact corneal endothelial proliferation and migration processes. Yet, these compounds have not been established as pharmacological alternatives to enhance corneal endothelial regeneration in addition to EK or DSO surgery for treating corneal decompensation. Our study, through an *in vitro* cell-based screening pipeline, has identified new compounds like ROCKi-2, Chroman-1, and SAR407899, that were not described in the context of corneal endothelial regeneration. We identified Chroman-1, exhibiting optimal effects at a low optimal concentration of 10 nM, as a promising repurposed compound for future hit-to-lead optimization to boost corneal endothelial regeneration. Furthermore, our study establishes a strong framework to stimulate a pharmacological-based research approach providing alternative strategies to donor-dependent therapies for corneal endothelial purposes.

CRedit authorship contribution statement

Bert Van den Bogerd: Supervision, Project administration, Conceptualization. **Hendrik Vercammen:** Writing – review & editing, Writing – original draft, Visualization, Validation, Project administration, Methodology, Investigation, Data curation, Conceptualization. **Martin Ondra:** Writing – review & editing, Visualization, Validation, Methodology, Investigation. **Jana Kotulova:** Writing – review & editing, Visualization, Supervision, Methodology, Formal analysis. **Edgar Cardenas De La Hoz:** Software, Data curation. **Charissa Witters:** Writing – review & editing, Validation, Investigation, Formal analysis, Data curation. **Katerina Jecmenova:** Writing – review & editing, Investigation, Data curation. **Maxim Le Compte:** Writing – review & editing. **Christophe Deben:** Writing – review & editing. **Sorcha Ní Dhubhghaill:** Writing – review & editing. **Carina Koppen:** Writing – review & editing. **Marián Hajdúch:** Writing – review & editing, Supervision, Methodology.

Declaration of Competing Interest

The authors declare that the research was conducted in the absence of any commercial or financial relationships that could be construed as a potential conflict of interest. All authors have read the journal's policy on conflicts of interest and authorship agreement.

Data availability

Data will be made available on request.

Acknowledgements

This study was supported by the organization called Funds Scientific Research Flanders (FWO) via the FWO-mandate grant (1S09722N) that HV received and an FWO fundamental research project (G073623N). This study was supported by the Ministry of Education, Youth and Sports of the Czech Republic (European Infrastructure for Translational Medicine — EATRIS-CZ, Project No. LM2023053) and the National Institute for Cancer Research — Program EXCELES, ID Project No. LX22NPO5102, Funded by the European Union — Next Generation EU. Furthermore, this research project was also supported by the Institute of Molecular and Translational Medicine (IMTM). We truly believe that this research project is an example of how interdisciplinary research and teamwork can be done in an international context.

References

- [1] K.M. Meek, C. Knupp, Corneal structure and transparency, *Prog. Retin Eye Res* 49 (2015) 1–16.
- [2] R.a.D.N, Noncommunicable diseases, sensory functions, disability and rehabilitation (SDR), World report on vision, W. H. Organ. (2019) 180.
- [3] M.O. Price, J.S. Mehta, U.V. Jurkunas, F.W. Price Jr., Corneal endothelial dysfunction: Evolving understanding and treatment options, *Prog. Retin Eye Res.* 82 (2021) 100904.
- [4] F. Aiello, G. Gallo Aflitto, F. Ceccarelli, M. Cesareo, C. Nucci, Global prevalence of fuchs endothelial corneal dystrophy (FECD) in adult population: a systematic review and meta-analysis, *J. Ophthalmol.* 2022 (2022) 3091695.
- [5] N. Okumura, N. Koizumi, Regeneration of the corneal endothelium, *Curr. Eye Res* 45 (3) (2020) 303–312.
- [6] G.H. Yam, X. Seah, N. Yusoff, M. Setiawan, S. Wahlig, H.M. Htoon, G.S.L. Peh, V. Kocaba, J.S. Mehta, Characterization of human transition zone reveals a putative progenitor-enriched niche of corneal endothelium, *Cells* 8 (10) (2019).
- [7] N.C. Joyce, Proliferative capacity of corneal endothelial cells, *Exp. Eye Res* 95 (1) (2012) 16–23.
- [8] T. Joko, A. Shiraishi, T. Kobayashi, Y. Ohashi, S. Higashiyama, Mechanism of proliferation of cultured human corneal endothelial cells, *Cornea* 36 (Suppl 1) (2017) S41–S45.
- [9] B. Van den Bogerd, S.N. Dhubhghaill, C. Koppen, M.J. Tassignon, N. Zakaria, A review of the evidence for *in vivo* corneal endothelial regeneration, *Surv. Ophthalmol.* 63 (2) (2018) 149–165.
- [10] J. Jewitt-Harris, Anything but the Eyes; An art-based investigation into why people won't donate their corneas after death., 2020. (<https://theophthalmologist.com/subspecialties/anything-but-the-eyes/>).
- [11] P. Gain, R. Jullienne, Z. He, M. Aldossary, S. Acquart, F. Cognasse, G. Thuret, Global survey of corneal transplantation and eye banking, *JAMA Ophthalmol.* 134 (2) (2016) 167–173.
- [12] M. Ang, A. Moriyama, K. Colby, G. Sutton, L. Liang, N. Sharma, J. Hjortdal, D. Shun, Chiu Lam, P.W. G, J. Armitage, S.M. J, Corneal transplantation in the aftermath of the COVID-19 pandemic: an international perspective, *Br. J. Ophthalmol.* 104 (11) (2020) 1477–1481.
- [13] G.F. Wilkinson, K. Pritchard, *In vitro* screening for drug repositioning, *J. Biomol. Screen* 20 (2) (2015) 167–179.
- [14] S. Pushpakom, F. Iorio, P.A. Eyers, K.J. Escott, S. Hopper, A. Wells, A. Doig, T. Guilliams, J. Latimer, C. McNamee, A. Norris, P. Sanseau, D. Cavalla, M. Pirmohamed, Drug repurposing: progress, challenges and recommendations, *Nat. Rev. Drug Discov.* 18 (1) (2019) 41–58.
- [15] V. Parvathaneni, N.S. Kulkarni, A. Muth, V. Gupta, Drug repurposing: a promising tool to accelerate the drug discovery process, *Drug Discov. Today* 24 (10) (2019) 2076–2085.
- [16] J.J. Hernandez, M. Pryszyk, L. Smith, C. Yanchun, N. Kurji, V.M. Shahani, S. V. Molinski, Giving drugs a second chance: overcoming regulatory and financial hurdles in repurposing approved drugs as cancer therapeutics, *Front Oncol.* 7 (2017) 273.
- [17] Y. Xi, P.F. Xu, Therapeutic potentials of fasudil in liver fibrosis, *World J. Gastroenterol.* 27 (45) (2021) 7859–7861.
- [18] Pankaj Kumar Singh, Inhibition of rho-associated coiled-coil containing protein kinases with belumosudil mesylate shows anti-tumor and immune modulatory properties in models of multiple myeloma, *Blood* 142 (2023).
- [19] J.A. Tran, U.V. Jurkunas, J. Yin, E.C. Davies, D.A. Sola-Del Valle, T.C. Chen, M. M. Lin, Netarsudil-associated reticular corneal epithelial edema, *Am. J. Ophthalmol. Case Rep.* 25 (2022) 101287.
- [20] L. Pan, et al., Legumain Is an Endogenous Modulator of Integrin alphavbeta3 Triggering Vascular Degeneration, Dissection, and Rupture, *Circulation* 145 (9) (2022) 659–674.
- [21] J. Nakata, Y. Akiba, J. Nihara, L. Thant, K. Eguchi, H. Kato, K. Izumi, M. Ohkura, M. Otake, Y. Kakihara, I. Saito, M. Saeki, ROCK inhibitors enhance bone healing by promoting osteoclastic and osteoblastic differentiation, *Biochem Biophys. Res. Commun.* 526 (3) (2020) 547–552.
- [22] T. Hamano, N. Shirafuji, S.H. Yen, H. Yoshida, N.M. Kanaan, K. Hayashi, M. Ikawa, O. Yamamura, Y. Fujita, M. Kuriyama, Y. Nakamoto, Rho-kinase ROCK inhibitors reduce oligomeric tau protein, *Neurobiol. Aging* 89 (2020) 41–54.
- [23] V.P. Rao, D.L. Epstein, Rho GTPase/Rho kinase inhibition as a novel target for the treatment of glaucoma, *BioDrugs* 21 (3) (2007) 167–177.
- [24] S. Kinoshita, K.A. Colby, F.E. Kruse, A close look at the clinical efficacy of rho-associated protein kinase inhibitor eye drops for fuchs endothelial corneal dystrophy, *Cornea* 40 (10) (2021) 1225–1228.
- [25] H. Vercammen, A. Miron, S. Oellerich, G.R.J. Melles, S. Ni Dhubhghaill, C. Koppen, B. Van, Den Bogerd, Corneal endothelial wound healing: understanding the regenerative capacity of the innermost layer of the cornea, *Transl. Res* 248 (2022) 111–127.
- [26] U. Schlotzer-Schrehardt, M. Zenkel, M. Strunz, A. Giessl, H. Schondorf, H. da Silva, G.A. Schmidt, M.A. Greiner, N. Okumura, N. Koizumi, S. Kinoshita, T. Tourtas, F. E. Kruse, Potential functional restoration of corneal endothelial cells in fuchs endothelial corneal dystrophy by rock inhibitor (Ripasudil), *Am. J. Ophthalmol.* 224 (2021) 185–199.
- [27] R. Karri, E.W. Chong, ROCK inhibitors in ophthalmology: a critical review of the existing clinical evidence, *Clin. Exp. Ophthalmol.* 51 (5) (2023) 472–483.
- [28] M. Esner, F. Meyenhofer, M. Bickle, Live-cell high content screening in drug development, *Methods Mol. Biol.* 1683 (2018) 149–164.
- [29] L. Xiao, D. Fan, H. Qi, Y. Cong, Z. Du, Defect-buffering cellular plasticity increases robustness of metazoan embryogenesis, *Cell Syst.* 13 (8) (2022) 615–630, e9.

- [30] C. Gambato, E. Longhin, A.G. Catania, D. Lazzarini, R. Parrozzani, E. Midena, Aging and corneal layers: an in vivo corneal confocal microscopy study, *Graefes Arch. Clin. Exp. Ophthalmol.* 253 (2) (2015) 267–275.
- [31] D.A. Van Valen, T. Kudo, K.M. Lane, D.N. Macklin, N.T. Quach, M.M. DeFelice, I. Maayan, Y. Tanouchi, E.A. Ashley, M.W. Covert, Deep learning automates the quantitative analysis of individual cells in live-cell imaging experiments, *PLoS Comput. Biol.* 12 (11) (2016) e1005177.
- [32] R.P. Bajaj, M.J. Flitsos, T. Pradeep, A.O. Eghrari, Peripheral-to-central ratio of Guttata: validity and reliability of an objective method to characterize severity of Fuchs endothelial corneal dystrophy, *Graefes Arch. Clin. Exp. Ophthalmol.* 259 (3) (2021) 685–690.
- [33] C. Deben, et al., OrBITS: a high-throughput, time-lapse, and label-free drug screening platform for patient-derived 3D organoids, *bioRxiv* (2021), 2021.09.09.459656.
- [34] S. Martinotti, E. Ranzato, Scratch wound healing assay, *Methods Mol. Biol.* 2109 (2020) 225–229.
- [35] B. Van den Bogerd, N. Zakaria, S. Matthyssen, C. Koppen, S. Ni, Dhubghaill, exploring the mesenchymal stem cell secretome for corneal endothelial proliferation, *Stem Cells Int* 2020 (2020) 5891393.
- [36] D. Kampik, M. Basche, A. Georgiadis, U.F.O. Luhmann, D.F. Larkin, A.J. Smith, R. R. Ali, Modulation of Contact Inhibition by ZO-1/ZONAB gene transfer-a new strategy to increase the endothelial cell density of corneal grafts, *Invest Ophthalmol. Vis. Sci.* 60 (8) (2019) 3170–3177.
- [37] X. Wang, Q. Zhou, C. Zhao, H. Duan, W. Li, C. Dong, Y. Gong, Z. Li, W. Shi, Multiple roles of FGF10 in the regulation of corneal endothelial wound healing, *Exp. Eye Res* 205 (2021) 108517.
- [38] J.A. Bonanno, Molecular mechanisms underlying the corneal endothelial pump, *Exp. Eye Res* 95 (1) (2012) 2–7.
- [39] C. Dong, D. Zou, H. Duan, X. Hu, Q. Zhou, W. Shi, Z. Li, Ex vivo cultivated retinal pigment epithelial cell transplantation for the treatment of rabbit corneal endothelial dysfunction, *Eye Vis.* 10 (1) (2023) 34.
- [40] S.P. Srinivas, Dynamic regulation of barrier integrity of the corneal endothelium, *Optom. Vis. Sci.* 87 (4) (2010) E239–E254.
- [41] M. Lawlor, I. Kerridge, Anything but the eyes: culture, identity, and the selective refusal of corneal donation, *Transplantation* 92 (11) (2011) 1188–1190.
- [42] M. Lawlor, I. Kerridge, R. Ankeny, T.A. Dobbins, F. Billson, Specific unwillingness to donate eyes: the impact of disfigurement, knowledge and procurement on corneal donation, *Am. J. Transpl.* 10 (3) (2010) 657–663.
- [43] M. Toro, T. Choragiewicz, C. Posarelli, M. Figus, R. Rejdak, C.-C.G. European, Early Impact of COVID-19 outbreak on the availability of cornea donors: warnings and recommendations, *Clin. Ophthalmol.* 14 (2020) 2879–2882.
- [44] H. Miyagi, S. Kim, J. Li, C.J. Murphy, S.M. Thomasy, Topical Rho-Associated Kinase Inhibitor, Y27632, Accelerates Corneal Endothelial Regeneration in a Canine Cryoinjury Model, *Cornea* 38 (3) (2019) 352–359.
- [45] K.E. Keller, S.K. Bhattacharya, T. Borras, T.M. Brunner, S. Chansangpetch, A. F. Clark, W.M. Dismuke, Y. Du, M.H. Elliott, C.R. Ethier, J.A. Faralli, T.F. Freddo, R. Fuchshofer, M. Giovingo, H. Gong, P. Gonzalez, A. Huang, M.A. Johnstone, P. L. Kaufman, M.J. Kelley, P.A. Knepper, C.C. Kopczynski, J.G. Kuchtey, R. W. Kuchtey, M.H. Kuehn, R.L. Lieberman, S.C. Lin, P. Liton, Y. Liu, E. Lutjen-Drecoll, W. Mao, M. Masis-Solano, F. McDonnell, C.M. McDowell, D.R. Overby, P. P. Pattabiraman, V.K. Raghunathan, P.V. Rao, D.J. Rhee, U.R. Chowdhury, P. Russell, J.R. Samples, D. Schwartz, E.B. Stubbs, E.R. Tamm, J.C. Tan, C.B. Toris, K.Y. Torrejon, J.A. Vranka, M.K. Wirtz, T. Yorio, J. Zhang, G.S. Zode, M.P. Fautsch, D.M. Peters, T.S. Acott, W.D. Stamer, Consensus recommendations for trabecular meshwork cell isolation, characterization and culture, *Exp. Eye Res.* 171 (2018) 164–173.
- [46] N. Okumura, Y. Okazaki, R. Inoue, K. Kakutani, S. Nakano, S. Kinoshita, N. Koizumi, Effect of the Rho-Associated Kinase Inhibitor Eye Drop (Ripasudil) on Corneal Endothelial Wound Healing, *Invest Ophthalmol. Vis. Sci.* 57 (3) (2016) 1284–1292.
- [47] E. Fernandez Lopez, S. Montolio-Marzo, C. Ortega Perez, M. Catalan Gomez, C. Peris Martinez, J.V. Pia Ludena, E. Chan, Descemet stripping only and ripasudil for the treatment of traumatic Descemet's membrane ruptures, *Eur. J. Ophthalmol.* 33 (4) (2023) NP13–NP18.
- [48] K. Numa, K. Imai, M. Ueno, K. Kitazawa, H. Tanaka, J.D. Bush, S. Teramukai, N. Okumura, N. Koizumi, J. Hamuro, C. Sotozono, S. Kinoshita, Five-Year Follow-up of First 11 patients undergoing injection of cultured corneal endothelial cells for corneal endothelial failure, *Ophthalmology* 128 (4) (2021) 504–514.
- [49] I. Popa-Burke, J. Russell, Compound precipitation in high-concentration DMSO solutions, *J. Biomol. Screen* 19 (9) (2014) 1302–1308.
- [50] M.Aa.A.C. Bray, *Advanced Assay Development Guidelines for Image-Based High Content Screening and Analysis*, Assay Guidance Manual, S. Markossian, et al. Bethesda (MD) (2004).
- [51] D.J. Colussi, M.A. Jacobson, Patient-derived phenotypic high-throughput assay to identify small molecules restoring lysosomal function in tay-sachs disease, *SLAS Discov.* 24 (3) (2019) 295–303.
- [52] G.S. Gibbons, H. Gould, V.M. Lee, A. Crowe, K.R. Brunden, Identification of small molecules and related targets that modulate tau pathology in a seeded primary neuron model, *J. Biol. Chem.* 299 (7) (2023) 104876.
- [53] M. Boncler, M. Rozalski, U. Krajewska, A. Podsedek, C. Watala, Comparison of PrestoBlue and MTT assays of cellular viability in the assessment of anti-proliferative effects of plant extracts on human endothelial cells, *J. Pharm. Toxicol. Methods* 69 (1) (2014) 9–16.
- [54] D. Bandyopadhyay, C. Gatzka, L.A. Donehower, E.E. Medrano, Analysis of cellular senescence in culture in vivo: the senescence-associated beta-galactosidase assay, *Curr. Protoc. Cell Biol.* 18 (2005), 18 9 1-18 9 9.
- [55] O. Braissant, M. Astasov-Frauenhoffer, T. Waltimo, G. Bonkat, A review of methods to determine viability, vitality, and metabolic rates in microbiology, *Front Microbiol* 11 (2020) 547458.
- [56] J. Van Hoorick, J. Delaey, H. Vercammen, J. Van Erps, H. Thienpont, P. Dubruel, N. Zakaria, C. Koppen, S. Van Vlierberghe, B. Van den Bogerd, Designer Descemet Membranes Containing PDLA and functionalized gelatins as corneal endothelial scaffold, *Adv. Health Mater.* 9 (16) (2020) e2000760.
- [57] P. Catala, N. Groen, J.A. Dehnen, E. Soares, A.J.H. van Velthoven, R. Nuijts, M. M. Dickman, V.L.S. LaPointe, Single cell transcriptomics reveals the heterogeneity of the human cornea to identify novel markers of the limbus and stroma, *Sci. Rep.* 11 (1) (2021) 21727.
- [58] A.N. Sheerin, S.K. Smith, K. Jennert-Burston, A.J. Brook, M.C. Allen, B. Ibrahim, D. Jones, C. Wallis, K. Engelmann, W. Rhys-Williams, R.G. Faragher, D. Kipling, Characterization of cellular senescence mechanisms in human corneal endothelial cells, *Aging Cell* 11 (2) (2012) 234–240.
- [59] O. Tornavaca, M. Chia, N. Dufton, L.O. Almagro, D.E. Conway, A.M. Randi, M. A. Schwartz, K. Matter, M.S. Balda, ZO-1 controls endothelial adherens junctions, cell-cell tension, angiogenesis, and barrier formation, *J. Cell Biol.* 208 (6) (2015) 821–838.
- [60] P. Goyal, A. Behring, A. Kumar, W. Siess, STK35L1 associates with nuclear actin and regulates cell cycle and migration of endothelial cells, *PLoS One* 6 (1) (2011) e16249.
- [61] S. Ueda, T. Tominaga, A. Ochi, A. Sakurai, K. Nishimura, E. Shibata, S. Wakino, M. Tamaki, K. Nagai, TGF-beta1 is involved in senescence-related pathways in glomerular endothelial cells via p16 translocation and p21 induction, *Sci. Rep.* 11 (1) (2021) 21643.
- [62] R. Lowe, N. Shirley, M. Bleackley, S. Dolan, T. Shafee, Transcriptomics technologies, *PLoS Comput. Biol.* 13 (5) (2017) e1005457.
- [63] R.F. Frausto, V.S. Swamy, G.S.L. Peh, P.M. Boere, E.M. Hanser, D.D. Chung, B. L. George, M. Morselli, L. Kao, R. Azimov, J. Wu, M. Pellegrini, I. Kurtz, J.S. Mehta, A.J. Aldave, Phenotypic and functional characterization of corneal endothelial cells during in vitro expansion, *Sci. Rep.* 10 (1) (2020) 7402.
- [64] M. Unbekandt, M.F. Olson, The actin-myosin regulatory MRCK kinases: regulation, biological functions and associations with human cancer, *J. Mol. Med. (Berl.)* 92 (3) (2014) 217–225.
- [65] G.S.L. Peh, F. Bandeira, D. Neo, K. Adnan, Y. Hartono, H.S. Ong, S. Naso, A. Venkatraman, J.A.P. Gomes, V. Kocaba, J.S. Mehta, Effects of Rho-Associated Kinase (Rock) Inhibitors (Alternative to Y-27632) on Primary Human Corneal Endothelial Cells, *Cells* 12 (9) (2023).